

What Makes an Aquaporin a Glycerol Channel? A Comparative Study of AqpZ and GlpF

Yi Wang,^{1,2} Klaus Schulten,^{1,2}
and Emad Tajkhorshid^{1,2,*}

¹Theoretical and Computational Biophysics Group
Beckman Institute for Advanced Science
and Technology
University of Illinois at Urbana-Champaign
Urbana, Illinois 61801

Summary

The recent availability of high-resolution structures of two structurally highly homologous, but functionally distinct aquaporins from the same species, namely *Escherichia coli* AqpZ, a pure water channel, and GlpF, a glycerol channel, presents a unique opportunity to understand the mechanism of substrate selectivity in these channels. Comparison of the free energy profile of glycerol conduction through AqpZ and GlpF reveals a much larger barrier in AqpZ (22.8 kcal/mol) than in GlpF (7.3 kcal/mol). In either channel, the highest barrier is located at the selectivity filter. Analysis of substrate-protein interactions suggests that steric restriction of AqpZ is the main contribution to this large barrier. Another important difference is the presence of a deep energy well at the periplasmic vestibule of GlpF, which was not found in AqpZ. The latter difference can be attributed to the more pronounced structural asymmetry of GlpF, which may play a role in attracting glycerol.

Introduction

Permeation of water across cellular membranes is facilitated by a family of transmembrane channels called aquaporins (AQPs) (Preston et al., 1992; Borgnia et al., 1999). These selective channels are present in all forms of life, including mammals, amphibia, insects, plants, and bacteria (Agre et al., 1998; Borgnia et al., 1999; Heynmann and Engel, 1999). In humans, 11 different AQPs have been characterized in various organs such as kidneys, eyes, and the brain. AQPs are fundamental to osmoregulation of a large variety of cells (Agre et al., 1998). Impaired function of AQPs has been associated with diseases such as nephrogenic diabetes insipidus and congenital cataract (Agre et al., 1998; Deen and van Os, 1998; Borgnia et al., 1999; Li and Verkman, 2001).

Water permeation is the best-characterized physiological function of AQPs. However, AQPs also participate in rather diverse cellular functions. For example, a subfamily of AQPs, called aquaglyceroporins, stereoselectively conducts small linear sugar molecules such as glycerol (Heller et al., 1980; Borgnia and Agre, 2001; Grayson et al., 2003). The *Escherichia coli* (*E. coli*) glycerol uptake facilitator GlpF is a prominent member of

this subfamily. Permeability of AQPs to small substrates other than water and glycerol, such as urea (Borgnia et al., 1999), nitrate (Ikeda et al., 2002), arsenite (Liu et al., 2002), and even ions (Yool and Weinstein, 2002), has been reported. Some AQPs may function as gas channels in cellular membranes; for instance, the tobacco aquaporin-1, NtAqp1, has been proposed to be a membrane CO₂ pore (Uehlein et al., 2003).

Crystallographic, atomic resolution structures of several AQPs have been solved. The first structure of an AQP was the one of human AQP1, which was solved using electron microscopy at a medium resolution (3.8 Å; Murata et al., 2000). Since the high-resolution (2.2 Å) structure of GlpF was first determined by X-ray crystallography (Fu et al., 2000), more AQP structures have been solved, including those of bovine AQP1 (2.2 Å; Sui et al., 2001) and *E. coli* AqpZ (2.5 Å; Savage et al., 2003), as well as sheep (3.0 Å; Gonen et al., 2004) and bovine (2.2 Å; Harries et al., 2004) AQP0. Among the structurally known AQPs, two functionally different AQPs, namely GlpF and AqpZ, are both derived from the same organism, *E. coli*. Despite their structural similarity, AqpZ is a pure water channel whereas GlpF is involved in the uptake of glycerol and other small sugars from the environment. Visual comparison of the two structures reveals an extremely high degree of homology between the two proteins. A thorough examination of the channels, as performed in this study, revealed that AqpZ forms a narrower, more hydrophilic pore than GlpF with a less pronounced periplasmic protrusion. Naturally, the question arises as to what determines the different substrate selectivity of the two AQPs. The present study addresses this question.

Water permeation in AQPs has been extensively studied by classical molecular dynamics (MD) simulations (Zhu et al., 2001; Jensen et al., 2001, 2002, 2003; de Groot et al., 2001; Tajkhorshid et al., 2002). Steered MD (SMD) and interactive MD (IMD) simulations have been used to study the conduction of glycerol and other linear sugar molecules through GlpF (Jensen et al., 2002; Grayson et al., 2003). Using Jarzynski's identity (Jarzynski, 1997b), a potential of mean force (PMF) associated with glycerol permeation through GlpF has been reconstructed (Jensen et al., 2002; Park et al., 2003; Park and Schulten, 2004). The obtained PMF has successfully described the pertinent minima and barriers along the channel (Jensen et al., 2002).

Water pores in AQPs strictly exclude protons, ions, and charged solutes while conducting water effectively (Sansom and Law, 2001). This remarkable property posed a long-standing puzzle because proton conduction can readily occur via the Grotthuss mechanism (de Grotthuss, 1806; Nagle and Morowitz, 1978; Schulten and Schulten, 1986; Agmon, 1995; Pomès and Roux, 1996; Zundel, 2000) through a hydrogen-bonded chain of water molecules, which had been proposed earlier and was revealed by MD simulations (Zhu et al., 2001; Jensen et al., 2001; de Groot et al., 2001; Tajkhorshid et al., 2002; Roux and Schulten, 2004; de Groot and Grubmüller, 2005) to exist in AQP channels. A novel

*Correspondence: emad@ks.uiuc.edu

²Lab address: <http://www.ks.uiuc.edu>

mechanism for proton exclusion was recognized by MD simulations of these channels (Tajkhorshid et al., 2002). The mechanism is based on an unusual configuration of water (bipolar configuration) inside the pore, which is controlled by highly tuned electrostatic forces of the protein environment and prevents proton conduction while permitting fast water permeation (Tajkhorshid et al., 2002). Several later computational studies applying different models confirmed the validity of this mechanism (de Groot et al., 2003; Chakrabarti et al., 2004; Ilan et al., 2004).

It is of interest and importance to understand what structural and dynamical properties provide an AQP with the ability of conducting glycerol, as in the case of GlpF, and when an AQP conducts exclusively water. AqpZ is a pure water channel, and does not conduct glycerol. However, by investigating an artificially induced passage of glycerol through the channel, one may study major barriers against the permeation of the substrate through the channel. In this study, using a fully hydrated, membrane-embedded model of tetrameric AqpZ (Figure 1), we have investigated the energetics associated with permeation of glycerol molecules through the channel, as induced by means of SMD. The simulations allowed us to calculate the energetics of glycerol passage through AqpZ using the protocol that had been applied to GlpF earlier (Jensen et al., 2002). The two free energy profiles can be directly compared to each other. The comparison provides useful information regarding the mechanism of permeation and presents a clear picture of structural and functional differences between the two channels.

The results show that the main barriers against the permeation of glycerol through AqpZ are steric in nature, mainly due to a narrower pore size of AqpZ, not only at the selectivity filter (SF) but overall along the entire channel. Furthermore, an attractive energy well, which was characterized at the periplasmic vestibule of GlpF in a previous study (Jensen et al., 2002), was not found in AqpZ. A key arginine lining the SF of AqpZ has been found in two distinct conformational states, one of which blocks the substrate flow through the channel, thus acting as a gate. Analysis of the orientation of water molecules and glycerol hydroxyl groups along the channel clearly shows that, similar to other AQPs (de Groot et al., 2001; Tajkhorshid et al., 2002; Jensen et al., 2003), a bipolar configuration of the permeating substrate is also present in AqpZ.

Results and Discussion

In this section, we will describe the main results of our MD and SMD simulations of AqpZ, including the observation of a bipolar, single file of water inside all monomers during the equilibration phase, and the calculation of the PMF for glycerol conduction through AqpZ.

Water Configuration inside the Pore

Previous MD simulations (Zhu et al., 2001; Jensen et al., 2001; de Groot et al., 2001; Tajkhorshid et al., 2002) of other AQPs, namely AQP1 and GlpF, have revealed that water molecules form a single file inside the constriction region of the pores, and that water permeation happens as a result of correlated displacements of

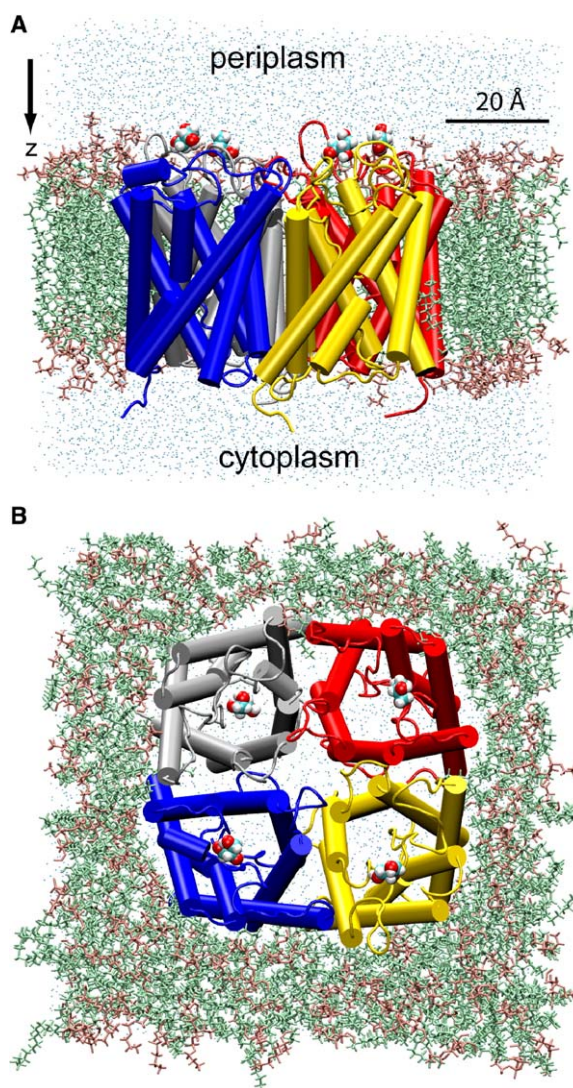


Figure 1. AqpZ Tetramer Embedded in a Hydrated POPE Membrane Side view (A) and top view from the periplasmic side (B). AqpZ monomers are shown in individually colored cartoon representations. One glycerol molecule (vdW representation) is positioned at the periplasmic side above each monomer and is pulled along the +z axis (from periplasm to cytoplasm) during the SMD simulations. The lipid head groups and the fatty acid parts are shown in purple and green, respectively. Some of the lipid molecules are omitted in (A) to provide a better view of the protein. Water molecules appear as blue points (only a fraction of water molecules is shown).

water molecules in this region. Furthermore, the configuration of water inside AQPs was found to be a unique one, in which water molecules flip at the center of the channel in order to align themselves to opposite electric fields generated by the protein in the two halves of the channel and to maximize the number of their hydrogen bonds (Tajkhorshid et al., 2002; Jensen et al., 2003). In other words, water molecules in the two halves of the single-file region adopt a bipolar orientation, with their oxygen atoms always facing the center of the channel from both entrances. A water molecule in the middle of the channel, which is involved in two hydrogen bonds with the conserved NPA (asparagine-

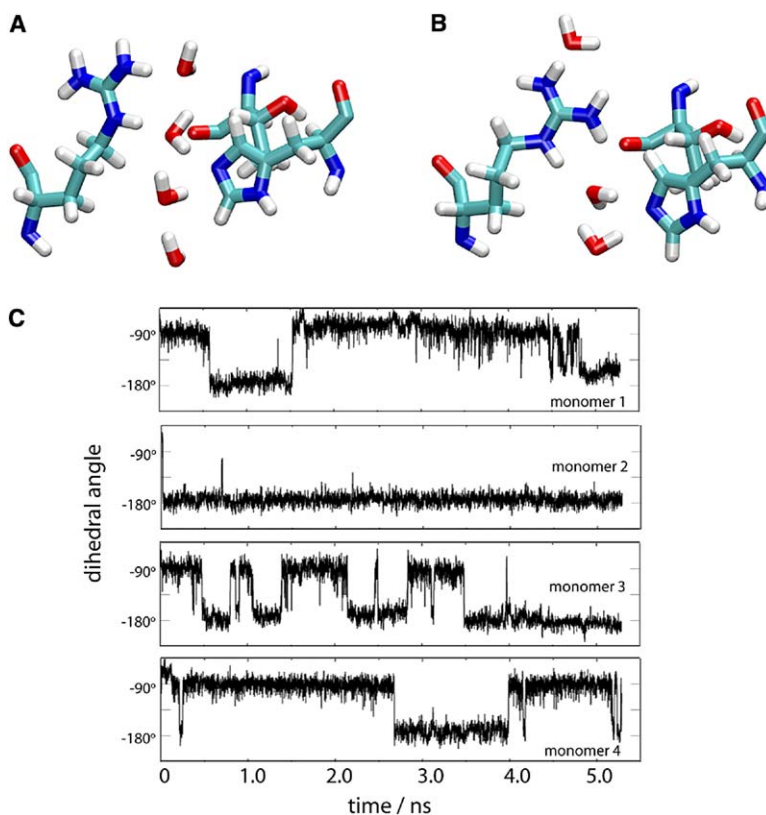


Figure 2. Two States of the Side Chain of Arg189

(A) Arg189 in the UP state and water molecules forming a single file.

(B) Arg189 in the DOWN state and the channel being blocked.

(C) Dihedral angle $C_{\beta}-C_{\gamma}-C_{\delta}-N_{\epsilon}$ of Arg189 of four monomers in the first 5 ns of equilibration.

Except for monomer 2, in which the side chain is always in the UP state, Arg189 in all monomers fluctuates between two stable states, UP and DOWN. SF residues His174 and Thr183 and water molecules in the SF region are shown in (A) and (B). The value of the mentioned dihedral angle is -172° in (A) and -87° in (B).

proline-alanine) motifs, assumes an almost orthogonal orientation relative to the membrane normal, linking the two oppositely oriented water half-chains. This bipolar ordering of single-file water “disrupts” a potential proton wire and, thereby, introduces a barrier against proton conduction (Tajkhorshid et al., 2002; Zhu and Schulten, 2003). The underlying mechanism for proton exclusion, which has been verified with different computational methodologies (Tajkhorshid et al., 2002; Jensen et al., 2003; de Groot et al., 2003; Chakrabarti et al., 2004; Ilan et al., 2004), is expected to apply to the entire AQP family. Our simulation of AqpZ provides another opportunity to test this hypothesis.

The crystal structure of AqpZ includes the coordinates of only five and three water oxygen atoms inside the pore region of protomers A and B, respectively. These water molecules are located very close to the NPA motifs in one protomer, and span the region of NPA and the SF in the other. However, they are completely disconnected from both the cytoplasmic and periplasmic bulk regions. Simulation of the system in a fully solvated environment and under constant pressure conditions in less than 100 ps resulted in the formation of a continuous single file of water inside all AqpZ monomers connecting water on the two sides of the membrane. Interestingly, single files of water molecules could not be formed in the first phase of the equilibration when the protein was fixed, and only after allowing the protein to undergo its natural dynamics could water molecules penetrate the channel and complete the gap between the bulk and water molecules buried deep inside the channel. This observation is a clear indication

of the importance of fluctuations of channel-lining residues on the conduction rate of water in AQPs. In contrast to some artificial water channels, such as carbon nanotubes (Hummer et al., 2001; Zhu and Schulten, 2003; Zhu et al., 2004), that merely provide a conduit for water, AQPs furnish hydrogen bond-forming groups that interact dynamically with water molecules. Thermal fluctuation of these groups has an accelerating effect on the recruitment of water molecules from the bulk and on the transfer of water molecules from one “binding” site to the next one.

As expected, water molecules in AqpZ exhibit a similar configuration to those found in other AQPs, that is, a clear bipolar ordering is discernible for single-file water molecules in all four monomers. A central water molecule forms direct H bonds with the NH_3^+ s of the two asparagine side chains of the NPA motifs and offers its two hydrogens for hydrogen bonding to the oxygen atoms of neighboring water molecules. The bipolar single file propagates through water-water hydrogen bonding from the NPA motifs to the two vestibules of the channel. The carbonyl groups of residues 59–62 and 182–185 on the two reentrant loops of AqpZ serve as additional H bond acceptors for the hydrogen atoms of water molecules, and along with the NPA motifs form a complete pathway for substrate transfer from one vestibule to another. The organization of AqpZ’s single file of water matches exactly the organization found in GlpF (Tajkhorshid et al., 2002).

At the SF, water molecules form frequent H bonds with the N_{ϵ} atom of His174 and the guanidinium group of Arg189 during the simulations. In comparison to the

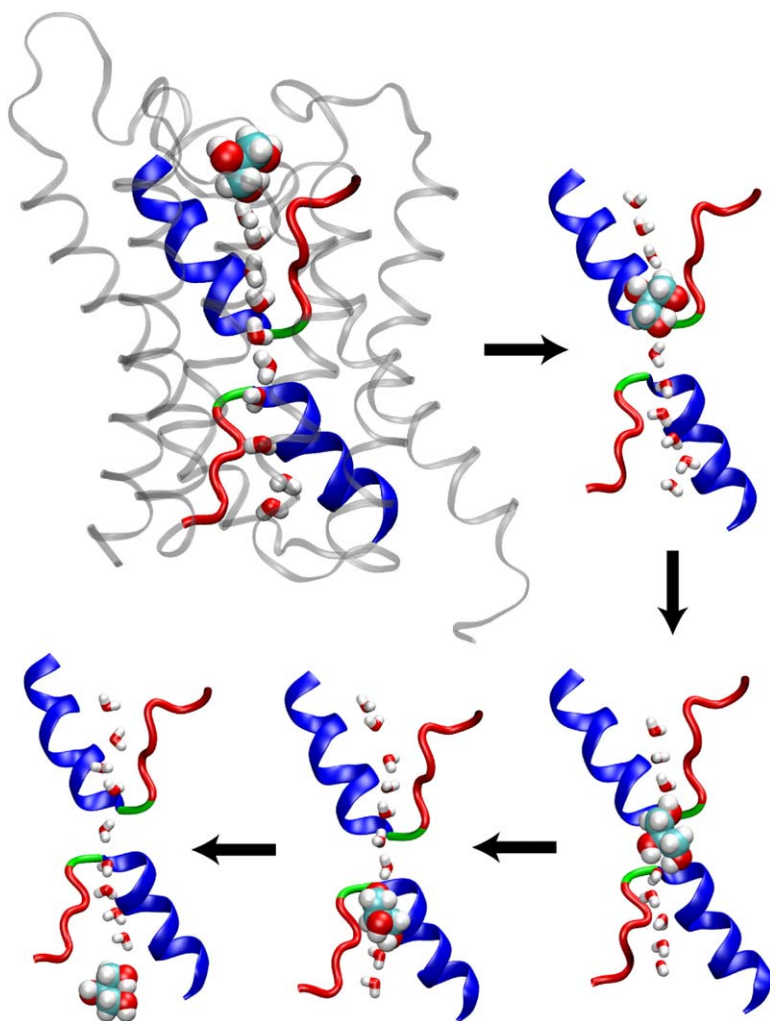


Figure 3. Representative Snapshots of cv-SMD Simulations, Showing a Monomer with Glycerol Permeating from the Periplasmic Vestibule to the Cytoplasmic Vestibule

The single file formed by glycerol and water is discernible. Water molecules adopt opposite orientations in the two halves of the channel. Hydroxyl groups of glycerol are in similar orientations as water molecules at the corresponding positions. Two reentrant loops are highlighted, the nonhelical parts in red, the asparagines of the NPA motifs in green, and the α -helical parts in blue. The rest of the monomer is shown in transparent gray in the first snapshot (left, top).

SF of GlpF, the SF of AqpZ is about 1.0 Å narrower in diameter and more hydrophilic, both factors likely contributing to AqpZ's impermeability to hydrophobic sugar molecules such as glycerol which present a larger and less flexible molecular species than water.

Gating of Arg189

The SF in AQPs is the narrowest part of the channel. In this region, the pore narrows down to 3.3 Å and 2.4 Å in diameter in GlpF and AqpZ, respectively. A highly conserved arginine side chain lines the SF in all AQPs. It is interesting that despite the quasi-2-fold symmetry of sequence and structure of AQPs, which seems to be the result of a gene duplication, this arginine only appears in one half of the protein, that is, only at the periplasmic half of the channel. A high degree of conservation of this side chain is a clear indication of its important role, but so far no study has implicated this residue in the structural stability of the protein, nor has anybody proposed a functional role for it.

During the first 5 ns of equilibration of AqpZ, the side chain of the SF arginine (Arg189 in AqpZ) alternated between two distinct states, as shown in Figure 2. In its "UP" state, the SF represents an open channel, and

a continuous single file of water molecules that freely permeated through the channel was maintained. The average value of the dihedral $C_{\beta}-C_{\gamma}-C_{\delta}-N_{\epsilon}$ in the UP state is -173° . In contrast, in the "DOWN" state, characterized by an average dihedral value of -88° , which occurred only transiently, but frequently, during the first phase of equilibration, the SF of the channel is completely occluded by this side chain. A persistent blocking event longer than 100 ps initiated further dehydration of the constriction region and water molecules of the broken single file started to leave the channel. As described in the Methods section, after constraining this side chain for 8 ns, the UP state became the dominant state, and no further flipping of the side chain was observed during the subsequent cf-SMD (cf, constant force) and cv-SMD (cv, constant velocity) simulations. However, the motion of this residue might be of importance in AQPs. So far, no regulatory and/or gating mechanism has been reported for water pores of AQPs. The length and the permanent charge of this side chain along with the observed fluctuation between a closed and an open channel make it a very good candidate for a possible gating mechanism in AQPs. Arginine side chains are very well known to function as voltage sen-

sors in voltage-gated channels. However, a voltage sensing mechanism seems to be unlikely in AQPs, as the displacement of the charged guanidinium group of the SF arginine during its transition between the UP and the DOWN states only amounts to about 3 Å along the membrane normal, that is, along the direction of the membrane electric field. In the presence of physiological membrane potentials (on the order of 100 mV), such a small displacement produces only a marginal preference for one of the two states. Obviously, further investigations are necessary to verify a gating role for the SF arginine and its mechanism. It is noteworthy that a similar blocking motion for the SF arginine has also been reported for AQP1 (Zhu et al., 2001). Furthermore, the two adopted conformations of this side chain in the two protomers of AqpZ's crystal structure (Savage et al., 2003) are also indicative of the flexibility of this side chain.

Steered Glycerol Permeation

Both cf-SMD and cv-SMD simulations were performed to compare glycerol permeation events through AqpZ and GlpF. The results obtained from the two methods complement each other. The cf-SMD method applies a constant force to one atom or a group of atoms, glycerol in this case, throughout the simulations. The residence time of glycerol in different regions inside the channel is indicative of barriers glycerol faces at every point along the channel. Selecting a suitable force to complete the passage within the available simulation time, but not faster, is not straightforward. Usually, forces on the order of 100–1000 pN are used in such simulations (Lu and Schulten, 2000; Isralewitz et al., 2001; Gao et al., 2003; Sotomayor et al., 2005). In the present simulations, a constant force of 400 pN applied to the CG3 atom of glycerol was not strong enough to make glycerol pass through the SF of AqpZ in 1.5 ns (data not shown). In contrast, in the same orientation, glycerol permeated readily through the GlpF channel under the same force during a 1 ns simulation (Jensen et al., 2002). The difference clearly suggests that AqpZ presents a significantly higher energy barrier against the permeation of glycerol than does GlpF.

A typical transport event of glycerol in cv-SMD simulations is illustrated through snapshots shown in Figure 3. A single file composed of water molecules and glycerol was maintained throughout the permeation event, in which glycerol used its hydroxyl groups to form H bonds with neighboring water molecules. The overall orientation of water molecules along the channel is similar to that in a pure water channel, that is, the orientation of the bipolar single-file type. Interestingly, we found that the hydroxyl groups of glycerol also experienced similar reorientation as water molecules when passing through the NPA region, as shown in Figure 3. Figure 4 shows the average orientation of glycerol hydroxyl groups at various regions along the channel axis in the form of an order parameter describing the angle between the dipole vector of individual OH groups and the membrane normal (the z axis). The results show a clear inversion of the hydroxyl dipole at the center of the channel that resembles closely the water dipole inversion in GlpF and AQP1 (de Groot et al., 2001; Tajkhorshid et al., 2002; Jensen et al., 2003).

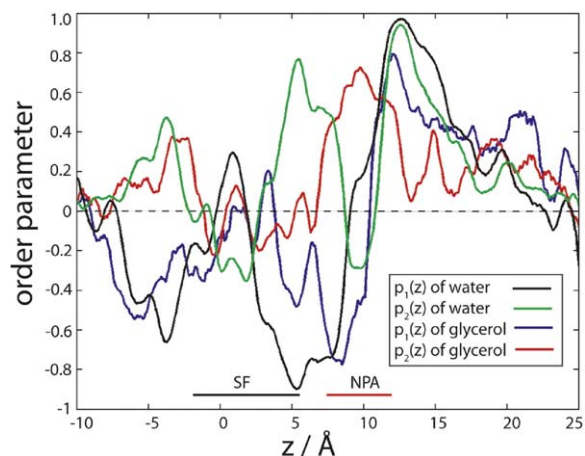


Figure 4. Average Orientation of Water and Hydroxyl Groups of Glycerol in cv-SMD Simulations

The order parameters $P_1(z) = \langle \cos\theta \rangle$ and $P_2(z) = 1/2 \langle 3\cos^2\theta - 1 \rangle$ are used to depict the hydroxyl groups' orientations, where θ is the angle between the membrane normal and the hydroxyl groups' dipole vector. The bipolar orientation of the hydroxyl groups in the two halves of the channel is clearly discernible.

Comparison of dipole orientation of water molecules and of hydroxyl groups of glycerol shows that, in general, hydroxyl groups of glycerol have smaller order parameters (c.f. Figure 4) than water molecules at the same relative positions along the channel, that is, they have a less pronounced orientational preference. The lower flexibility of glycerol hydroxyl groups, which results in a diminished value of the $\langle \cos\theta \rangle$ order parameter (see Figure 4), can be attributed to the fact that glycerol's hydroxyl groups are covalently bound to the rest of the molecule and, therefore, are orientationally more restricted than water dipoles. As such, glycerol's OH bonds cannot assume orientations with extreme values such as $\theta = 0, \pi$. This limitation also explains the low probability of finding a glycerol hydroxyl group in an orthogonal orientation to the channel axis at the center of the channel, as can be deduced from the value of $P_2(z)$ for glycerol OH groups in this region.

Energetics of Glycerol Conduction

In an earlier study (Jensen et al., 2002), we determined the PMF of glycerol permeation through GlpF. To compare the results of Jensen et al. (2002) with the PMF of glycerol conduction through AqpZ, we have determined the PMF associated with an enforced glycerol permeation through AqpZ employing the same protocols and parameters, such as spring constant and pulling velocity, as used for GlpF in Jensen et al. (2002). However, due to the channel of AqpZ being significantly narrower than that of GlpF, especially in the SF region, we had to further slow down the pulling speed in the constriction region of the channel to avoid too large forces and bringing the system too far off equilibrium, a problem that arose already for the PMF reconstruction for glycerol permeating through GlpF (Jensen et al., 2002). In the present case, the pulling velocities were lowered to

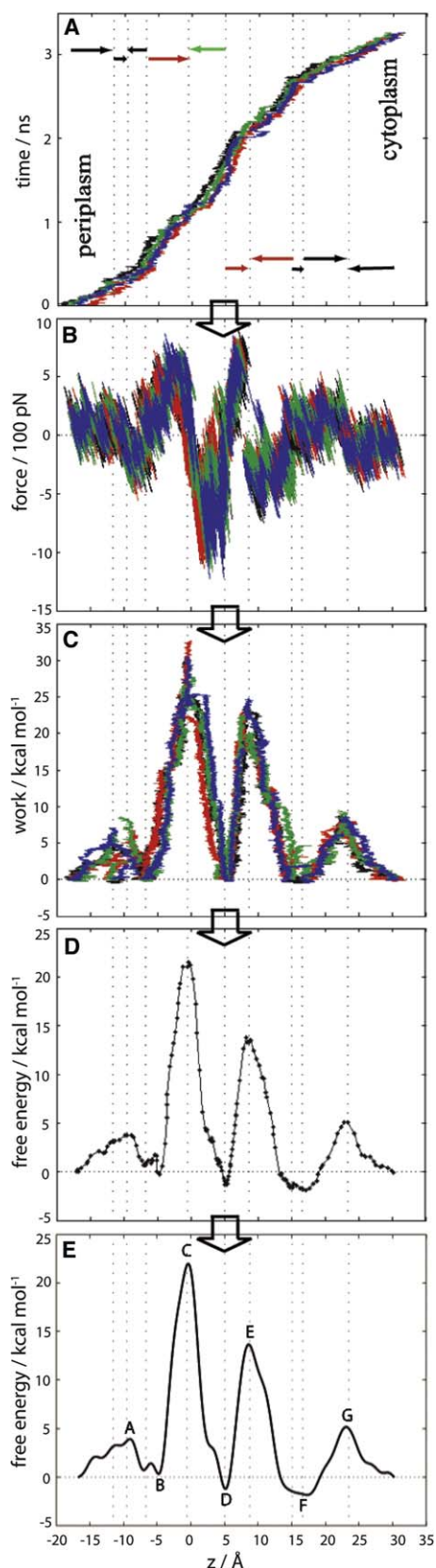


Figure 5. Reconstruction of the PMF of Glycerol Permeation through AqpZ

The procedure is illustrated in five consecutive steps in the order (A)–(E).

0.01 Å/ps and 0.015 Å/ps as indicated in Figure 5 by the green and red arrows, respectively.

The resulting PMF along the AqpZ channel is shown in Figure 5E. One can see that the PMF reaches its maximum with a peak value of 22.8 kcal/mol at the SF. This significant free energy barrier of AqpZ could result from two possible mechanisms, increased hydrophilicity and/or a reduced pore size compared with GlpF. Analysis of the interactions between the glycerol and the channel suggests that the steric barrier introduced by a narrower pore size of AqpZ is the main contribution to the free energy barrier. As shown in Figure 6, throughout the constriction region of the channel, AqpZ has a much narrower pore than GlpF. Although the pore of AqpZ is narrower than GlpF almost everywhere in the constriction region ($-7 \text{ \AA} \leq z \leq 15 \text{ \AA}$), the most severe restriction happens at the SF where the pore diameter of AqpZ measures only 2.4 Å, which is about 1.0 Å smaller than found in GlpF. Compared to GlpF, this is a very significant contraction of the pore size for a region that is already rather narrow for glycerol passage in GlpF. Consequently, in order to accommodate the glycerol molecule, the narrow pore of AqpZ has to widen at this region. Indeed, major conformational changes of residues lining the SF were observed during the enforced permeation of glycerol through this region. Several examples of such conformational changes are presented in Figure 7.

As shown in Figure 7A, with the glycerol entering from the periplasmic vestibule, His174 at the SF was pushed away and the aromatic ring of Phe43 had to rotate $\sim 60^\circ$ to avoid a strong steric clash with glycerol. The side chains of Arg189 and His174 were both pushed upward. The only favorable interactions between glycerol and the protein at this time are an H bond between the carbonyl group of Thr183 (not shown) and one of the hydroxyl groups (HO3) of the glycerol, as well as an H bond between the H_ϵ atom of Arg189 and the middle oxygen atom of the glycerol. Another representative conformational change occurred to side chains of His174 and Arg189 in a different monomer with the glycerol being pulled from the periplasmic side. As shown in Figure 7B, the glycerol's presence forced the aromatic ring of His174 to flip about 90° and pushed the side chain of Arg189 out of the way. Another significant perturbation of the SF region is shown in Figure 7C. In order to accommodate the glycerol molecule, both Arg189 and His174 were forced to move their side chains. The HO1 atom of the glycerol formed an H bond with the N_ϵ atom of His174. In keeping with the known impermeability of AqpZ to

- (A) Trajectory of the center of mass of glycerol molecules.
- (B) External force applied to atoms being pulled.
- (C) External work calculated from (A) and (B) using Equation 2.
- (D) PMF in each section calculated according to Equation 6.
- (E) Combined PMF.

Data from different monomers are colored differently (black, red, green, and blue) in (A)–(C). Arrows in (A) denote pulling directions, and their colors indicate the pulling velocity: blue for 0.03 Å/ps, green for 0.015 Å/ps, and red for 0.01 Å/ps. Positions along the channel axis z were measured relative to the position of the C_α atom of Thr183 as the reference.

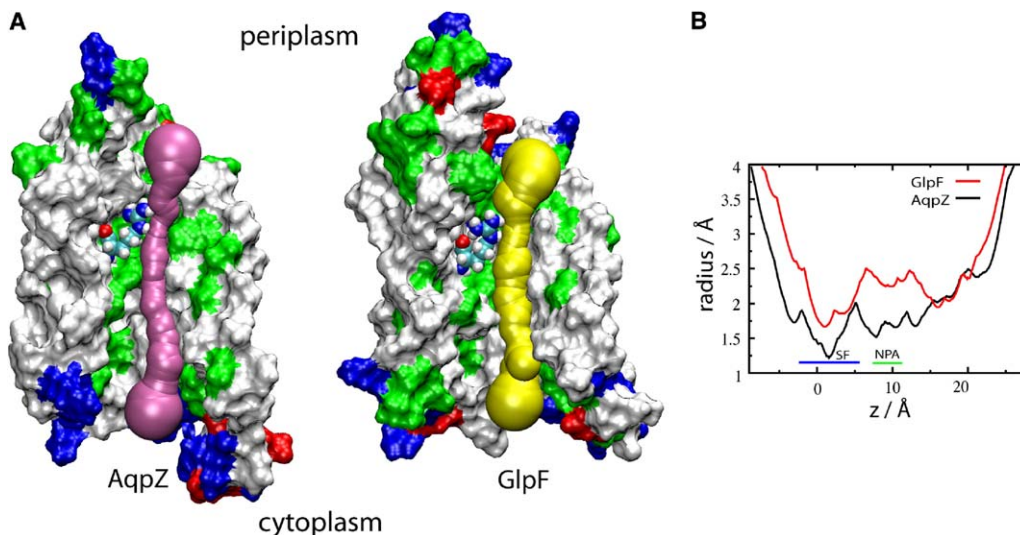


Figure 6. Comparison of the Pores of AqpZ and GlpF

(A) The radii of the pores were calculated using the program HOLE (Smart et al., 1993) and shown in mauve and yellow. AqpZ (residues 1–7, 9–13, 66–188, and 190–231) and GlpF (residues 1–13, 15–17, 67–205, and 208–259) are shown in surface representation, colored by residue type (red, acidic; blue, basic; green, polar; white, nonpolar) with the exception of the arginine at SF, which is shown in vdW representation. (B) Radii of the pores in AqpZ and GlpF along the channel axis.

glycerol and the very high barrier against glycerol passage through this region, qualitative examination of the SF clearly shows that this part of the channel is not designed to accommodate large molecules such as glycerol, and any penetration of glycerol into this region should result in a large perturbation of the side chains lining the channel. This observation is in sharp contrast

to the observed permeation of glycerol through the SF of GlpF (Jensen et al., 2002), in which case, despite the presence of an energy barrier at the SF, only minor widening of the channel is needed for the passage of glycerol. Comparison of the glycerol-saturated (Fu et al., 2000) and glycerol-free (Tajkhorshid et al., 2002) structures of GlpF also indicates that the presence of

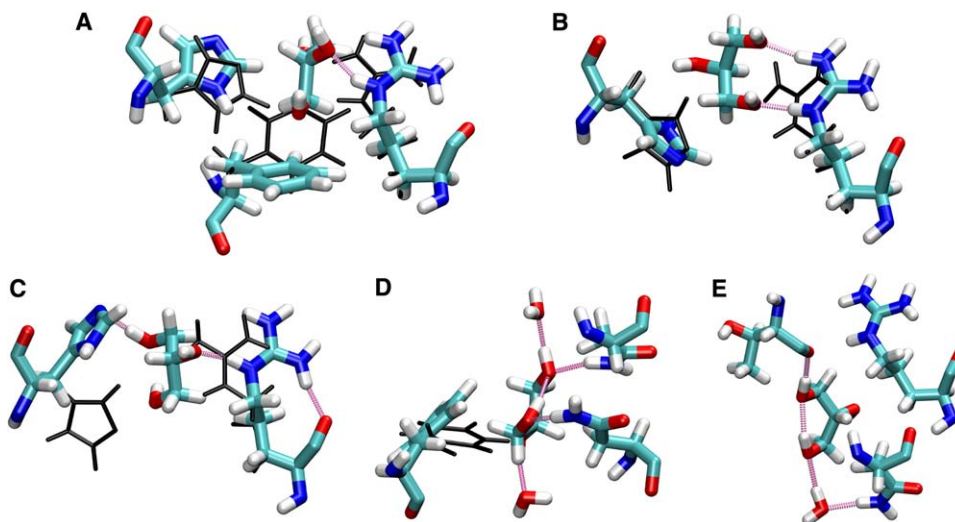


Figure 7. Snapshots of Glycerol from cv-SMD Simulations

(A and B) Glycerol at the SF (pulled along the +z direction).
(C) Glycerol at the SF (pulled along the -z direction).
(D) Glycerol at the NPA motifs.
(E) Glycerol at the position between the SF and NPA motifs.

(A)–(C) correspond to the local maxima C of the PMF shown in Figure 5E. (D) and (E) correspond to the local maximum D and minimum E, respectively. The original positions of side chains lining the channel before glycerol entered the region are shown in a dark line representation, illustrating conformational changes induced by the passage of glycerol. Hydrogen bonds are shown in dashed lines colored in mauve.

glycerol in the SF introduces only a minute widening of the channel.

Another major energy barrier against glycerol permeation through AqpZ is observed at the NPA region ($6.5 \text{ \AA} \leq z \leq 12.0 \text{ \AA}$). This local maximum of the PMF can also be attributed mostly to steric effects. Although the pore is significantly wider in this region than near the SF, we note that the size of the pore is still small, in fact comparable to the pore size of the SF in GlpF (Figure 6). The diameter of AqpZ in the NPA region is $\sim 3.0 \text{ \AA}$, which is significantly smaller than the corresponding value of 4.5 \AA in GlpF, and even smaller than the SF of GlpF with a diameter of 3.3 \AA . Major conformational changes of side chains in this region were also occasionally observed in our SMD simulations during the passage of glycerol through this region. One such occasion is shown in Figure 7D, where the aromatic ring of Phe145 at the NPA region was forced to flip by about 60° to allow passage of the glycerol.

The local minimum of the PMF located between the SF and NPA regions is connected with an increase in the pore size (Figure 6). This increase provides glycerol with more room for subtle conformational changes that increases the number of favorable interactions with the protein. As shown in one of the snapshots taken from the simulations (Figure 7E), the backbone of glycerol adopted a position that could match the shape of the channel closely. No large structural distortion of channel-lining residues was observed during the passage of glycerol in this region. A series of H bonds were formed between the carbonyl group of Thr183, two hydroxyl groups of the glycerol, and a water molecule.

At the two vestibules of AqpZ, a small free energy barrier was observed in the PMF. These barriers are much smaller than those observed inside the constriction region of the channel and cannot be easily interpreted in terms of interactions between the substrate and the channel, as no significant favorable interaction between glycerol and the protein was observed in this region. Loss of entropy and partial desolvation of glycerol during the transition from bulk water to the channel vestibule contribute to the rise of the PMF in these regions.

Comparison of Glycerol Permeation through AqpZ and GlpF

The main difference between glycerol permeation through GlpF and AqpZ seems to be the height of the main energy barrier controlling channel conduction. The largest free energy barrier in the PMF of glycerol permeation through AqpZ is found to be 22.8 kcal/mol , which is about three times higher than the highest barrier against glycerol permeation in GlpF (7.3 kcal/mol ; Jensen et al., 2002). The calculated barrier against glycerol permeation might seem too high in GlpF, which is a glycerol channel, and one may suspect that computational errors are the main source for the calculated high barrier. However, the Arrhenius activation energy inferred from measurement of glycerol permeability of GlpF-reconstituted liposomes is reported to be $9.6 \pm 1.6 \text{ kcal/mol}$ (Borgnia and Agre, 2001), which is in good agreement with the calculated value of 7.3 kcal/mol (Jensen et al., 2002).

The location of the highest barriers at the narrowest part of the channel in both cases already hints at the importance of steric interactions in the height of these barriers. While the increased hydrophilicity of the SF in AqpZ could be viewed as one reason for the reduced permeability of the channel for glycerol, our results suggest that the main effect underlying the large barrier in this region is the significantly reduced pore radius in AqpZ. It is interesting that even at the NPA region, the pore of AqpZ is narrow enough (with a diameter of 3.0 \AA) to introduce a significant barrier to glycerol.

Another major difference between the two channels concerns the presence of a -4 kcal/mol energy well in the PMF of GlpF at the periplasmic vestibule of the channel (Jensen et al., 2002). The asymmetric positioning of this attractive well in GlpF, that is, only at the periplasmic vestibule, has been attributed to the asymmetric structure of the channel (Jensen et al., 2002) and may be important for an optimal rate of substrate permeation (Lu et al., 2003). AqpZ does not provide an attractive site for glycerol at any of its vestibules. Comparison of the sequences of the two proteins clearly shows that the two periplasmic loops responsible for the asymmetric structure of GlpF are both significantly shorter in AqpZ (Figure 8). As such, AqpZ has a smaller periplasmic domain, which may account for the lack of an attractive free energy well in its PMF.

Conclusions

Selectivity in membrane channels is of fundamental importance for biological cells. The present comparative investigation of two structurally and genetically highly similar, but functionally distinct AQPs from the same species presents a prime opportunity to reveal the physical basis of selectivity of membrane channels in atomic detail. The simulations suggest that Arg189 acts as a gate of AqpZ. When Arg189 is stabilized in its open position, the channel fills with water molecules that adopt a bipolar single-file arrangement, inverted at the NPA motifs. The arrangement is the same as found in GlpF and prevents leakage of protons through AqpZ and GlpF.

The SMD method was used to enforce glycerol permeation through AqpZ in order to analyze the interaction of substrate and protein and to calculate the energetics of the event. The calculated energy barrier of glycerol permeation is about three times larger in AqpZ than in GlpF, in keeping with the impermeability of the channel to glycerol in AqpZ. Analysis of trajectories clearly shows a strong repulsive steric interaction between glycerol and the channel, mainly at the SF, but also in the NPA region. We conclude that the smaller pore radius of AqpZ and steric effects are the main sources of differences in permeability of GlpF and AqpZ. The smaller pore size along the entire channel cannot be convincingly explained only by implicating channel-lining residues. We propose that other residues beyond the pore region that determine the overall configuration and relative position of helices in AqpZ and GlpF are responsible for the difference. Successful identification of such residues may suggest mutations to convert a water channel to a glycerol channel or vice versa and can be tested experimentally.

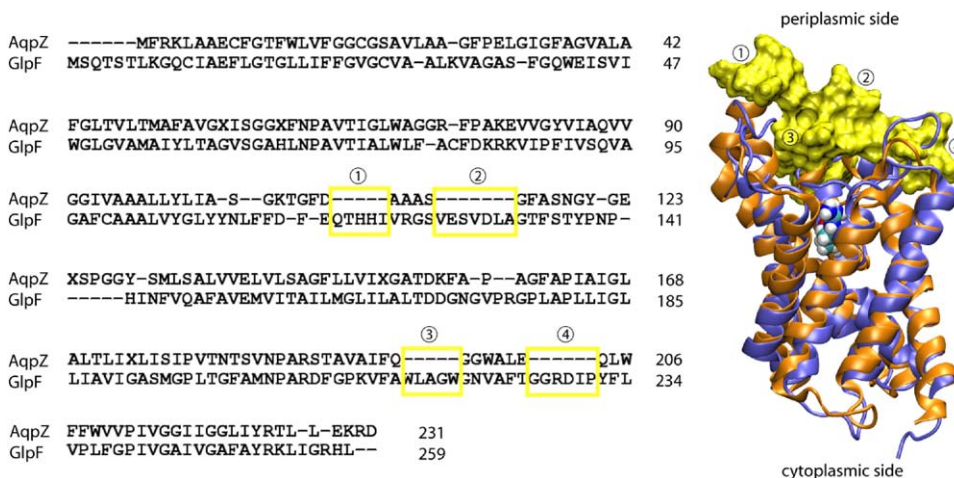


Figure 8. Comparison of Sequences and Structures of GlpF and AqpZ

Left: Sequence comparison of AqpZ and GlpF based on structural alignment of the two AQPs. Right: Structural alignment of the two channels with AqpZ in purple and GlpF in orange. GlpF's periplasmic loops that are missing in AqpZ (highlighted in yellow in the sequence) are shown in yellow surface representation. The structural alignment is done by the VMD Multiple Alignment plugin (O'Donoghue and Luthey-Schulten, 2005) based on the STAMP algorithm (Russell and Barton, 1992).

Another major difference between the free energy profiles of glycerol permeation through GlpF and AqpZ is the lack of an attractive free energy well in AqpZ. We propose that the more pronounced asymmetric structure of GlpF leading to a periplasmic vestibule of low energy serves GlpF by increasing the probability of recruiting a nonabundant substrate from the environment.

Experimental Procedures

In this section, the details of modeling membrane-embedded AqpZ and protocols as well as conditions used for our simulations will be presented.

Modeling

The crystal structure of *E. coli* AqpZ was obtained from the Protein Data Bank (PDB), entry 1RC2 (Savage et al., 2003). The PDB file contains two protomers, from which protomer A was used to build the system simulated here. A tetramer of AqpZ was generated with VMD (Humphrey et al., 1996) using the transformation matrices provided in the PDB file. The same transformation matrices were also applied to the crystallographically solved water molecules, except for a symmetry-related water molecule (water 1057), which was used without replication in building the tetramer. Missing side chains of residues Arg3, Glu31, Ser104, Arg230, and Asp231, as well as missing hydrogen atoms, were added using the program VMD (Humphrey et al., 1996; plugin PSFGEN). Titratable side chains were simulated in their default titration state, that is, all Glu and Asp residues with a negative charge, all Lys and Arg side chains with a positive charge, and all other side chains with zero charge. Using this titration scheme the protein is electrically neutral, and there was no need to add counterions to ensure the electroneutrality of the system. However, as will be described later, we opted to simulate the system in a solution with an ionic concentration of 100 mM, which better represents the natural environment of the protein.

A partially hydrated patch of 16:0/18:1 c9-palmitoylethanolamine (POPE) lipid bilayer was used to model the *E. coli* cell membrane. Initially, a 100 Å by 100 Å bilayer patch was built using the MEMBRANE plugin of VMD, with the membrane normal aligned along the z axis. The bilayer contained 282 POPE lipids and 4430 water molecules hydrating the head groups of the lipids. The AqpZ tetramer was then superimposed on this partially hy-

drated lipid bilayer. Surface tyrosine residues at the periphery of the tetramer were used to adjust the position of the tetramer along the membrane normal. All lipid and water molecules with heavy atoms closer than 0.8 Å to any atom of the protein were removed. Two 15 Å layers of water were then added using the SOLVATE plugin of VMD, in order to fully hydrate the system; 12 sodium and 12 chloride ions were added using the AUTOIONIZE plugin of VMD, generating a 100 mM ionic concentration. The final system, which is shown in Figure 1, contains 71,081 atoms: 13,525 AqpZ atoms, 19,625 lipid atoms, 37,872 water atoms, 12 sodium ions, and 12 chloride ions.

The system was first minimized for 5000 steps and simulated for about 300 ps at constant temperature (310 K) and pressure (1 atm) with all protein atoms fixed. Then the protein was released and the whole system equilibrated for 5 ns under the same conditions. During this phase, we noticed that the side chain of Arg189, which lines the channel in the periplasmic half of the pore, exhibited wild fluctuations in three of the four monomers; the side chain of this arginine alternates between two states in which the C_{β} - C_{γ} - C_{δ} - N_{ϵ} dihedral angle adopts an average value of about -173° and -88° , respectively, with the channel transiently blocked in the latter state. In order to prevent the blockage of the channel by this side chain, the mentioned dihedral angle was constrained to -173° by introducing an additional potential energy term for χ , namely, $V = k_{\chi}[1 + \cos(n\chi - \delta)]$, with $k_{\chi} = 14$ kcal/mol, $n = 1$, $\delta = 6.6^{\circ}$. The system was then equilibrated further for ~ 8 ns. This protocol resulted in a stable conformation of the arginine side chain. Indeed, in the following 8 ns equilibration and subsequent SMD simulations of the system, which were performed without the dihedral constraint, no blockage of the channel was observed. The structure of AqpZ after the equilibration was close to the crystal structure, exhibiting an rmsd of 1.8 Å for C_{α} atoms.

SMD Simulations

In order to study glycerol permeation through AqpZ with SMD, four glycerol molecules were added to the system. A glycerol molecule was placed at the periplasmic side of each monomer of the equilibrated system, at least 5 Å away from the protein. Water molecules within 5 Å of the glycerol molecules were removed. The new system, containing 70,507 atoms, was then minimized for 5000 steps and equilibrated for 150 ps with one of the terminal carbon atoms (CG3) of each glycerol being constrained along the z axis to keep glycerol at the same distance from the protein during the initial phase of simulation.

Constant force (cf) SMD simulations were carried out by applying a constant force (400 pN) along the z axis to one of the terminal carbon atoms (CG3) of each glycerol. When pulled at the CG3 atom, the glycerol enters the channel in the same orientation as found in the crystal structure (Fu et al., 2000) and assumed in earlier simulations (Jensen et al., 2002) of GlpF. The pulling started at the periplasmic side of AqpZ and proceeded along the +z direction (see Figure 1A).

Following Jensen et al. (2002), constant velocity (cv) SMD simulations were performed to reconstruct the so-called potential of mean force (PMF) using Jarzynski's identity (Jarzynski, 1997a; Park et al., 2003; Park and Schulten, 2004). For this purpose the pore region was divided into ten sections. cv-SMD simulations were completed independently in each section by attaching one of the terminal carbon atoms (CG3 for pulling along the +z direction, and CG1 for pulling along the -z direction) to a harmonic constraint moving with a constant velocity. The pulling velocity was set to 0.03 Å/ps for most of the sections. In the constriction region (-7 Å ≤ z ≤ 15 Å) of the channel, where the selectivity filter and the NPA motifs reside (see Figure 4), smaller velocities were chosen (0.01 Å/ps for 0 Å ≤ z ≤ 5 Å, and 0.015 Å/ps for -7 Å ≤ z ≤ 0 Å and for 5 Å ≤ z ≤ 15 Å). A large spring constant k (k = 150 pN/Å) was used to ensure that the pulled atoms follow the constraint closely (δz = √k_BT/k = 0.53 Å), a condition known as the stiff spring approximation and required for an efficient application of Jarzynski's identity (Park and Schulten, 2004). An even larger spring constant of 400 pN/Å was used for the region 0 Å ≤ z ≤ 5 Å where the channel is the narrowest. For each section, the starting configuration was prepared by a 150 ps equilibration with the glycerol's CG1 or CG3 atoms constrained to their initial positions. The C_α atoms of four residues distant from the pore, namely Phe2, Ala72, Gly83, and Thr225, were constrained with a spring constant of 69.5 pN/Å during the SMD simulations to counterbalance the external force applied to glycerol molecules and to prevent the overall translation of the system.

For all MD and SMD simulations, the program NAMD2 (Kalé et al., 1999) and the CHARMM27 parameter set (Schlenkrich et al., 1996; MacKerell et al., 1998) were used. Assuming periodic boundary conditions, the particle mesh Ewald method (Darden et al., 1993) with a grid density of at least 1/Å³ was employed for computation of electrostatic forces without cutoff. All simulations were performed with a time step of 1 fs. Langevin dynamics was used to keep the temperature constant (damping coefficient 5 ps⁻¹). During SMD simulations, glycerol molecules were not coupled to the temperature bath. A Langevin piston (Feller et al., 1995) was employed to maintain the pressure at 1 atm in all simulations.

Reconstruction of PMF

SMD simulations clearly present nonequilibrium circumstances. The PMF, however, describes the energetics of an equilibrium system (Park et al., 2003; Park and Schulten, 2004). It applies rather well to native conduction in GlpF and AqpZ because the respective processes take place close to equilibrium conditions. In order to connect nonequilibrium and equilibrium regimes, that is, to obtain the PMF from SMD simulations, one can use Jarzynski's identity (Jarzynski, 1997a). For a classical mechanical system, characterized through a control variable λ and altered between two states with λ = λ₀ and λ = λ₁, respectively, the identity states that the free energy change, ΔG(λ₀ → λ₁), and the work done to the system in an SMD simulation, W(λ₀ → λ₁), are related through

$$e^{-\beta\Delta G(\lambda_0 \rightarrow \lambda_1)} = \langle e^{-\beta W(\lambda_0 \rightarrow \lambda_1)} \rangle \quad (1)$$

where ⟨...⟩ denotes an average over many simulations. ΔG(λ₀ → λ₁) corresponding to an equilibrium situation represents here the PMF. In our cv-SMD simulations, the channel-glycerol system is subjected to a time-dependent potential ΔU(z,t) = (1/2)k(z - z₀ - vt)², where k is the spring constant, v is the pulling velocity, and z and z₀ are the current and initial position of the atom being pulled, respectively. Here the control variable λ_j is λ_j = z₀ + vt_j. Then the external work applied to glycerol is

$$W(t) = - \int_0^t dt' kv(z - z_0 - vt') \quad (2)$$

For N trajectories (n = 1, ..., N), W_n(t) is the corresponding work calculated with Equation 2. We use all N trajectories to carry out the average ⟨...⟩ in the Jarzynski identity. Because we employ a stiff spring, the work W can be assumed to be Gaussian distributed, which simplifies the computation of the exponential average as discussed in Park and Schulten (2004). Each trajectory was divided into time windows of width Δt (Δt = 20 ps). In the time window j, the average position ⟨z̄(j)⟩ of the atoms being pulled in N trajectories was calculated according to

$$\langle \bar{z}(j) \rangle = \frac{1}{N} \sum_n \Delta t^{-1} \int_j dt z(t) \quad (3)$$

where ∫_jdt denotes the integral over the jth time window and z(t) the time dependence of z in the n-th system simulated. The average work ⟨W̄(j)⟩ done for N trajectories is

$$\langle \bar{W}(j) \rangle = \frac{1}{N} \sum_n \bar{W}_n(j) \quad (4)$$

where

$$\bar{W}_n(j) = \int_j \frac{dt}{\Delta t} \left[W_n(t) - \frac{k}{2} (\langle \bar{z}(j) \rangle - z_0 - vt(j))^2 \right] \quad (5)$$

with

$$\bar{t}(j) = \Delta t^{-1} \int_j dt t.$$

Within the stiff spring approximation, the free energy can be expressed through the second-order cumulant expansion (Jensen et al., 2002; Park and Schulten, 2004):

$$G(\langle \bar{z}(j) \rangle) = \langle \bar{W}(j) \rangle - \frac{\beta}{2} [\langle \bar{W}(j)^2 \rangle - \langle \bar{W}(j) \rangle^2] \quad (6)$$

where

$$\langle \bar{W}(j)^2 \rangle = \frac{1}{N} \sum_n \bar{W}_n(j)^2.$$

The PMF for the channel-glycerol system was finally constructed by combining the sectional PMFs through a Fourier series involving a linear combination of sine functions as described in Jensen et al. (2002). The entire procedure of the PMF reconstruction is illustrated in Figure 5.

Acknowledgments

This work is supported by National Institutes of Health grants P41-RR05969 and R01-GM067887. The authors gladly acknowledge supercomputer time provided by the Pittsburgh Supercomputer Center and the National Center for Supercomputing Applications via National Resources Allocation Committee grant MCA93S028.

Received: March 30, 2005

Revised: April 30, 2005

Accepted: May 6, 2005

Published: August 9, 2005

References

- Agmon, N. (1995). The Grotthuss mechanism. Chem. Phys. Lett. 244, 456–462.
- Agre, P., Bonhivers, M., and Borgnia, M.J. (1998). The aquaporins, blueprints for cellular plumbing systems. J. Biol. Chem. 273, 14659–14662.
- Borgnia, M.J., and Agre, P. (2001). Reconstitution and functional comparison of purified GlpF and AqpZ, the glycerol and water channels from *Escherichia coli*. Proc. Natl. Acad. Sci. USA 98, 2888–2893.
- Borgnia, M., Nielsen, S., Engel, A., and Agre, P. (1999). Cellular and molecular biology of the aquaporin water channels. Annu. Rev. Biochem. 68, 425–458.

- Chakrabarti, N., Tajkhorshid, E., Roux, B., and Pomès, R. (2004). Molecular basis of proton blockage in aquaporins. *Structure* 12, 65–74.
- Darden, T., York, D., and Pedersen, L. (1993). Particle mesh Ewald. An $N\text{-log}(N)$ method for Ewald sums in large systems. *J. Chem. Phys.* 98, 10089–10092.
- Deen, P.M.T., and van Os, C.H. (1998). Epithelial aquaporins. *Curr. Opin. Cell Biol.* 10, 435–442.
- de Groot, B.L., and Grubmüller, H. (2005). The dynamics and energetics of water permeation and proton exclusion in aquaporins. *Curr. Opin. Struct. Biol.* 15, 1–8.
- de Groot, B.L., Engel, A., and Grubmüller, H. (2001). A refined structure of human aquaporin-1. *FEBS Lett.* 504, 206–211.
- de Groot, B.L., Frigato, T., Helms, V., and Grubmüller, H. (2003). The mechanism of proton exclusion in the aquaporin-1 water channel. *J. Mol. Biol.* 333, 279–293.
- de Grotthuss, C.J.T. (1806). On the decomposition of water and dissolved bodies by means of galvanic electricity. *Ann. Chim.* LVIII, 54–74.
- Feller, S.E., Zhang, Y.H., Pastor, R.W., and Brooks, B.R. (1995). Constant pressure molecular dynamics simulation—the Langevin piston method. *J. Chem. Phys.* 103, 4613–4621.
- Fu, D., Libson, A., Miercke, L.J.W., Weitzman, C., Nollert, P., Krucinski, J., and Stroud, R.M. (2000). Structure of a glycerol conducting channel and the basis for its selectivity. *Science* 290, 481–486.
- Gao, M., Craig, D., Lequin, O., Campbell, I.D., Vogel, V., and Schulten, K. (2003). Structure and functional significance of mechanically unfolded fibronectin type III1 intermediates. *Proc. Natl. Acad. Sci. USA* 100, 14784–14789.
- Gonen, T., Sliz, P., Kistler, J., Cheng, Y., and Walz, T. (2004). Aquaporin-0 membrane junctions reveal the structure of a closed water pore. *Nature* 429, 193–197.
- Grayson, P., Tajkhorshid, E., and Schulten, K. (2003). Mechanisms of selectivity in channels and enzymes studied with interactive molecular dynamics. *Biophys. J.* 85, 36–48.
- Harries, W.E.C., Akhavan, D., Miercke, L.J.W., Khademi, S., and Stroud, R. (2004). The channel architecture of aquaporin 0 at a 2.2-angstrom resolution. *Proc. Natl. Acad. Sci. USA* 101, 14045–14050.
- Heller, K.B., Lin, E.C., and Wilson, T.H. (1980). Substrate specificity and transport properties of the glycerol facilitator of *Escherichia coli*. *J. Bacteriol.* 144, 274–278.
- Heynmann, J.B., and Engel, A. (1999). Aquaporins: phylogeny, structure, and physiology of water channels. *News Physiol. Sci.* 14, 187–193.
- Hummer, G., Rasaiah, J.C., and Noworyta, J.P. (2001). Water conduction through the hydrophobic channel of a carbon nanotube. *Nature* 414, 188–190.
- Humphrey, W., Dalke, A., and Schulten, K. (1996). VMD—visual molecular dynamics. *J. Mol. Graph.* 14, 33–38.
- Ikeda, M., Beitz, E., Kozono, D., Guggino, W.B., Agre, P., and Yasui, M. (2002). Characterization of aquaporin-6 as a nitrate channel in mammalian cells. Requirement of pore-lining residue threonine 63. *J. Biol. Chem.* 277, 39873–39879.
- Ilan, B., Tajkhorshid, E., Schulten, K., and Voth, G.A. (2004). The mechanism of proton exclusion in aquaporin channels. *Proteins* 55, 223–228.
- Israelowitz, B., Baudry, J., Gullingsrud, J., Kosztin, D., and Schulten, K. (2001). Steered molecular dynamics investigations of protein function. *J. Mol. Graph. Model.* 19, 13–25.
- Jarzynski, C. (1997a). Equilibrium free-energy differences from nonequilibrium measurements: a master equation approach. *Phys. Rev. E* 56, 5018–5035.
- Jarzynski, C. (1997b). Nonequilibrium equality for free energy differences. *Phys. Rev. Lett.* 78, 2690–2693.
- Jensen, M.Ø., Tajkhorshid, E., and Schulten, K. (2001). The mechanism of glycerol conduction in aquaglyceroporins. *Structure* 9, 1083–1093.
- Jensen, M.Ø., Park, S., Tajkhorshid, E., and Schulten, K. (2002). Energetics of glycerol conduction through aquaglyceroporin GlpF. *Proc. Natl. Acad. Sci. USA* 99, 6731–6736.
- Jensen, M.Ø., Tajkhorshid, E., and Schulten, K. (2003). Electrostatic tuning of permeation and selectivity in aquaporin water channels. *Biophys. J.* 85, 2884–2899.
- Kalé, L., Skeel, R., Bhandarkar, M., Brunner, R., Gursoy, A., Krawetz, N., Phillips, J., Shinozaki, A., Varadarajan, K., and Schulten, K. (1999). NAMD2: greater scalability for parallel molecular dynamics. *J. Comput. Phys.* 151, 283–312.
- Li, J., and Verkman, A.S. (2001). Impaired hearing in mice lacking aquaporin-4 water channels. *J. Biol. Chem.* 276, 31233–31237.
- Liu, Z., Shen, J., Carbrey, J.M., Mukhopadhyay, R., Agre, P., and Rosen, B.P. (2002). Arsenite transport by mammalian aquaglyceroporins AQP7 and AQP9. *Proc. Natl. Acad. Sci. USA* 99, 6053–6058.
- Lu, H., and Schulten, K. (2000). The key event in force-induced unfolding of titin's immunoglobulin domains. *Biophys. J.* 79, 51–65.
- Lu, D., Grayson, P., and Schulten, K. (2003). Glycerol conductance and physical asymmetry of the *Escherichia coli* glycerol facilitator GlpF. *Biophys. J.* 85, 2977–2987.
- MacKerell, A.D., Jr., Bashford, D., Bellott, M., Dunbrack, R.L., Jr., Evanseck, J.D., Field, M.J., Fischer, S., Gao, J., Guo, H., Ha, S., et al. (1998). All-atom empirical potential for molecular modeling and dynamics studies of proteins. *J. Phys. Chem. B* 102, 3586–3616.
- Murata, K., Mitsuoka, K., Hirai, T., Walz, T., Agre, P., Heymann, J.B., Engel, A., and Fujiyoshi, Y. (2000). Structural determinants of water permeation through aquaporin-1. *Nature* 407, 599–605.
- Nagle, J.F., and Morowitz, H.J. (1978). Molecular mechanisms for proton transport in membranes. *Proc. Natl. Acad. Sci. USA* 75, 298–302.
- O'Donoghue, P., and Luthey-Schulten, Z. (2005). Evolutionary profiles derived from the QR factorization of multiple structural alignments gives an economy of information. *J. Mol. Biol.* 346, 875–894.
- Park, S., and Schulten, K. (2004). Calculating potentials of mean force from steered molecular dynamics simulations. *J. Chem. Phys.* 120, 5946–5961.
- Park, S., Khalili-Araghi, F., Tajkhorshid, E., and Schulten, K. (2003). Free energy calculation from steered molecular dynamics simulations using Jarzynski's equality. *J. Chem. Phys.* 119, 3559–3566.
- Pomès, R., and Roux, B. (1996). Structure and dynamics of a proton wire: a theoretical study of H^+ translocation along the single-file water chain in the gramicidin A channel. *Biophys. J.* 71, 19–39.
- Preston, G.M., Carroll, T.P., Guggino, W.B., and Agre, P. (1992). Appearance of water channels in *Xenopus* oocytes expressing red cell CHIP28 protein. *Science* 256, 385–387.
- Roux, B., and Schulten, K. (2004). Computational studies of membrane channels. *Structure* 12, 1343–1351.
- Russell, R.B., and Barton, G. (1992). Multiple protein sequence alignment from tertiary structure comparison: assignment of global and residue confidence levels. *Proteins* 14, 309–323.
- Sansom, M.S.P., and Law, R.J. (2001). Membrane proteins: aquaporins—channels without ions. *Curr. Biol.* 11, R71–R73.
- Savage, D.F., Egea, P.F., Robles-Colmenares, Y., O'Connell, J.D., III, and Stroud, R.M. (2003). Architecture and selectivity in aquaporins: 2.5 Å X-ray structure of aquaporin z. *PLoS Biol.* 1, 334–340.
- Schlenkrich, M., Brickmann, J., MacKerell, A.D., Jr., and Karplus, M. (1996). Empirical potential energy function for phospholipids: criteria for parameter optimization and applications. In *Biological Membranes: A Molecular Perspective from Computation and Experiment*, K.M. Merz and B. Roux, eds. (Boston: Birkhauser), pp. 31–81.
- Schulten, Z., and Schulten, K. (1986). Proton conduction through proteins: an overview of theoretical principles and applications. *Methods Enzymol.* 127, 419–438.
- Smart, O., Goodfellow, J., and Wallace, B. (1993). The pore dimensions of gramicidin A. *Biophys. J.* 65, 2455–2460.
- Sotomayor, M., Corey, D.P., and Schulten, K. (2005). In search of the hair-cell gating spring: elastic properties of ankyrin and cadherin repeats. *Structure* 13, 669–682.

Sui, H., Han, B.-G., Lee, J.K., Walian, P., and Jap, B.K. (2001). Structural basis of water-specific transport through the AQP1 water channel. *Nature* 414, 872–878.

Tajkhorshid, E., Nollert, P., Jensen, M.Ø., Miercke, L.J.W., O'Connell, J., Stroud, R.M., and Schulten, K. (2002). Control of the selectivity of the aquaporin water channel family by global orientational tuning. *Science* 296, 525–530.

Uehlein, N., Lovisolio, C., Siefritz, F., and Kaldenhoff, R. (2003). The tobacco aquaporin NtAQP1 is a membrane CO₂ pore with physiological functions. *Nature* 425, 734–737.

Yool, A.J., and Weinstein, A.M. (2002). New roles for old holes: ion channel function in aquaporin-1. *News Physiol. Sci.* 17, 68–72.

Zhu, F., and Schulten, K. (2003). Water and proton conduction through carbon nanotubes as models for biological channels. *Biophys. J.* 85, 236–244.

Zhu, F., Tajkhorshid, E., and Schulten, K. (2001). Molecular dynamics study of aquaporin-1 water channel in a lipid bilayer. *FEBS Lett.* 504, 212–218.

Zhu, F., Tajkhorshid, E., and Schulten, K. (2004). Collective diffusion model for water permeation through microscopic channels. *Phys. Rev. Lett.* 93, 224501.

Zundel, G. (2000). Hydrogen bonds with large proton polarizability and proton transfer processes in electrochemistry and biology. *Adv. Chem. Phys.* 111, 1–217.